

# WAVE-VORTEX INTERACTIONS IN THE ATMOSPHERE, AND CLIMATE PREDICTION

Onno Bokhove

*Numerical Analysis and Computational Mechanics, Department of Applied Mathematics  
IMPACT, University of Twente, P.O. Box 217, Enschede, The Netherlands*

`o.bokhove@math.utwente.nl`

**Abstract** Can we construct an accurate atmospheric climate model with a balanced model representing its fluid mechanics, and with dissipative as well as non-dissipative parameterization schemes for the gravity-wave activity? To address this question, we focus our attention on a  $1\frac{1}{2}$ -layer atmospheric model with an isentropic troposphere and isothermal stratosphere. We investigate parcel dynamics in a hybrid Eulerian-Lagrangian formulation, potential vorticity conservation, static stability, linear modes and the concept of balanced flow; and briefly discuss wave-vortex interactions and recent advances in numerical solution techniques.

**Keywords:** hybrid Eulerian-Lagrangian fluid parcel dynamics, linear modes, balanced models, gravity waves, weather and climate prediction

## Introduction

Numerical weather and climate prediction is complicated because only the flow scales larger than at least  $\sim 10 \times 10 \times 1 \text{ km}^3$  can be resolved to date. When we use the (inviscid) primitive Navier-Stokes equations on these scales, the commonly used (semi-Lagrangian) numerical schemes implicitly filter all acoustic waves and some of the gravity-wave (GW) motion. The rapid small-scale three-dimensional turbulence is then certainly not resolved. Consequently, also the feedback of the unresolved wave and (quasi-two-dimensional) turbulent motions on the large-scale dynamics requires parameterization.

A lot of attention has been paid to simplified or balanced versions of the primitive equations, in which preservation of the conservation laws (of the inviscid dynamics) such as mass, energy and potential vorticity (PV) has been advocated to enhance the stability of these so-called ba-

lanced models. The large-scale flow is generally close to hydrostatic and geostrophic balance; the former due to the anisotropy of horizontal and vertical scales and the latter due to the rapid rotation of the Earth, both in these balanced models (by default) and the numerical integration schemes used. Consequently, one has a choice to use either the primitive equations or balanced models.

Birner et al. (2002) observed that vertical temperature profiles are nearly constant in the stratosphere with a distinct kink at the tropopause between the troposphere and stratosphere. To analyze several properties of atmospheric flows, we therefore derive a conceptual model of the atmosphere with an isentropic troposphere and isothermal stratosphere, where the entropy or potential temperature  $\theta$  and temperature  $T$  are constant, respectively. Subsequently, we illustrate the concept of balance by deriving a balanced model describing only the vortical motion from this so-called “ $\theta$ - $T$ -model”.

A novel derivation of this  $\theta$ - $T$ -model from the three-dimensional Euler equations, using a combination of asymptotic methods and physical simplifications, is given in the framework of a hybrid Eulerian-Lagrangian description of a fluid parcel (Section 1). This hybrid formulation of the Euler equations (Dixon and Reich, 2004) describes the Hamiltonian dynamics of each parcel as a dynamical system with six degrees of freedom with the internal and potential energy as function of space and time. The formulation is passive when this function is given. In contrast, an integral equation for the density using the Jacobian between Eulerian and Lagrangian space links the dynamics of all fluid parcels into a dynamically consistent continuum.

In the linearized  $\theta$ - $T$ -model, three time derivatives (or four in the parcel framework) in the model give rise to a pair of fast GW modes and one slow geostrophic mode, whose eigen-periods are separated in time on the  $f$ -plane. However, the dynamics are nonlinear and there may be a conversion of energy and momentum between these slow and fast modes. In Section 2 (i.e., Fig. 4), this is illustrated in simulations of the nonlinear dynamics initialized by a linear mode at finite amplitude, in which a simple hydraulic, dissipative wave-breaking parameterization is used.

In the nonlinear dynamics, the slow modes survive approximately on a slow manifold of lower dimension. Balanced models of vortical dynamics describe the slow motion on a slow manifold (Section 3), on which the dimension of phase space is reduced by two thirds (or half in the parcel framework) due to the removal of the pair of (fast) GW modes. Within the Eulerian-Lagrangian framework of parcel dynamics, we illustrate the derivation of (Hamiltonian) balanced models using two velo-

city constraints which arise in asymptotic expansions in a relevant small parameter (such as the Rossby or Froude number). These constraints define the reduction of the phase space to the slow or slaving manifold. We compare balanced and unbalanced trajectories in simplified simulations in Fig. 1(b). The generation of gravity waves by instabilities of a balanced flow, or the absorption of gravity waves by the nearly balanced mean flow through wave-vortex interactions indicate, however, that the slow manifold is not an exact manifold (Bühler and McIntyre, 2003; Vanneste and Yavneh, 2004).

In balanced models, these unbalanced GW effects can only be included by explicitly parameterizing the gravity waves. Likewise, in numerical weather and climate prediction small-scale, unresolved gravity waves require parameterization. We finish by briefly discussing idealized wave-vortex interactions and some recently developed numerical schemes for geophysical flows (Sections 4 and 5), and their relevance to General Circulation Models (GCMs).

## 1. Eulerian-Lagrangian Dynamics of Fluid Parcels

### Three-dimensional compressible Euler equations

Consider Newton's equations of motion for a fluid parcel with position  $\mathbf{x} = (x, y, z)^T$  and velocity  $\mathbf{u} = (u, v, w)^T$  [ $(\cdot)^T$  denotes the transpose] in a rotating reference frame with rotation vector  $\boldsymbol{\Omega}$

$$\frac{d\mathbf{x}}{dt} = \mathbf{u} = \frac{\partial H_{3D}}{\partial \mathbf{u}}, \quad \frac{d\theta}{dt} = 0 \quad \text{and} \quad (1)$$

$$\frac{d\mathbf{u}}{dt} = -\theta \nabla \Pi - \nabla \phi - 2\boldsymbol{\Omega} \times \mathbf{u} = -\frac{\partial H_{3D}}{\partial \mathbf{x}} - 2\boldsymbol{\Omega} \times \frac{\partial H_{3D}}{\partial \mathbf{u}} \quad (2)$$

with the parcel energy (extending Frank and Reich, 2003)

$$H_{3D}(\mathbf{x}, \mathbf{u}, \theta, t) = |\mathbf{u}|^2/2 + \theta \Pi(\mathbf{x}, t) + \phi(\mathbf{x}), \quad (3)$$

three-dimensional gradient  $\nabla$ ; external potential  $\phi$ , *e.g.*,  $\phi = gz$ ; potential temperature  $\theta = T(p/p_r)^{-\kappa}$ ; temperature  $T(\mathbf{x}, t)$ ; pressure  $p(\mathbf{x}, t)$  and reference pressure  $p_r$ ; and Exner function  $\Pi = c_p(p/p_r)^\kappa$  for an ideal gas  $p = \rho RT$  with density  $\rho(\mathbf{x}, t)$ , gas constant  $R$ , specific heat at constant pressure  $c_p$ , and  $\kappa = R/c_p$ . Note that  $\theta \nabla \Pi = (1/\rho) \nabla p$ , so that (2) attains its usual form (Dixon and Reich, 2004). We can write (1)–(3) as a non-canonical Hamiltonian system  $dq/dt = J \partial H_{3D} / \partial q$  with state vector  $q = (x, y, z, u, v, w, \theta)^T$  and a skew-symmetric tensor  $J$ . The state vector  $q$  is a function of time and fluid labels  $\mathbf{a} = (a, b, c)^T =$

$(a_1, a_2, a_3)^T$ , so  $q = q(\mathbf{a}, t)$ . If the parcel energy is a function of  $q$  and  $t$ , then (1)–(3) is non-autonomous.

The continuum character of the fluid, albeit hidden in the representation (1)–(3), appears through the density

$$\begin{aligned} \rho(\mathbf{x}, t) &= \int_D \rho(\mathbf{x}', t) \delta(\mathbf{x} - \mathbf{x}') dx' dy' dz' \\ &= \int_{D_0} \rho_0(\mathbf{a}) \delta(\mathbf{x} - \mathbf{x}'(\mathbf{a}, t)) da db dc \end{aligned} \quad (4)$$

with  $\mathbf{x}' = \mathbf{x}'(\mathbf{a}, t)$  in a domain  $D$  or  $D_0$ , since the Jacobian between label and position space is proportional to the inverse density

$$\rho_0(\mathbf{a})/\rho(\mathbf{x}, t) = \det |\partial \mathbf{x} / \partial \mathbf{a}|. \quad (5)$$

Hence, an element of mass  $dm$  relates to the density as follows:

$$dm = \rho(\mathbf{x}, t) dx dy dz = \rho_0(\mathbf{a}) da db dc. \quad (6)$$

A common choice is  $\rho(\mathbf{x}, 0) = \rho_0(\mathbf{a})$  and  $\mathbf{x}(\mathbf{a}, 0) = \mathbf{a}$ . The system (1)–(4) is closed and represents the fluid as a continuum. From (1), (4) and (5), we can derive the continuity equation

$$d\rho(\mathbf{x}, t)/dt = \partial_t \rho(\mathbf{x}, t) + \mathbf{u} \cdot \nabla \rho(\mathbf{x}, t) = -\rho(\mathbf{x}, t) \nabla \cdot \mathbf{u}(\mathbf{x}, t). \quad (7)$$

**Similarity to 2D vorticity dynamics.** We note that this hybrid description is akin to the (more familiar) situation in inviscid, incompressible, two-dimensional vorticity dynamics, where the passive or kinematic advection of each fluid parcel is described by a given stream function  $\psi(x, y, t)$  as Hamiltonian with horizontal coordinates  $\mathbf{x}_h = (x, y)^T$  and time  $t$ . Thus,  $dx/dt = u = -\partial\psi/\partial y$  and  $dy/dt = v = \partial\psi/\partial x$ . In contrast, a dynamically consistent formulation appears when the vorticity  $\omega = \nabla_h^2 \psi$  is conserved on each fluid parcel and linked to the continuum of parcels using

$$\omega(x, y, t) = \int_{D_0} \omega_0(a, b) \delta(\mathbf{x}_h - \mathbf{x}'_h(a, b, t)) da db$$

with domain  $D_0$ , delta function  $\delta(\cdot)$ , parcel position  $\mathbf{x}'_h(a, b, t)$ , and  $\omega_0(a, b)$  denoting the initial distribution of vorticity on parcels identified by labels  $a$  and  $b$ . Given  $\omega$  on each parcel, we calculate  $\psi$ . Hence, the dynamical description is closed, since incompressibility yields  $dx dy = da db$ . With  $\mathbf{v} = (u, v)^T$  and gradient  $\nabla_h$  in the horizontal direction, we find  $d\omega/dt = \partial\omega/\partial t + \mathbf{v} \cdot \nabla_h \omega = 0$ .

**Static stability.** To illustrate the formulation of the hybrid parcel dynamics, parcel oscillations in a static atmosphere with given parcel energy  $H_{3D} = |\mathbf{u}|^2/2 + \theta\Pi(z) + gz$  are shown in Fig. 1(a). We choose  $\Pi = \Pi(z)$  with potential temperature  $\theta = \theta_g(z)$  in its thermodynamics to satisfy hydrostatic balance  $\theta_g(z)\partial\Pi/\partial z = -g$ . Hence, we find  $d^2z'/dt^2 = -N^2z'$  for small amplitude oscillations with  $z' = z - z_r$  and a reference level  $z_r$ . Oscillations are then stable with Brunt–Väisälä frequency  $N$ , when  $N^2 = [g(d\theta_g/dz)/\theta_g]_{z=z_r} > 0$ , neutral when  $N^2 = 0$ , and unstable when  $N^2 < 0$ . Note that  $\theta$  is conserved on each parcel of air and generally different from  $\theta_g(z)$ .

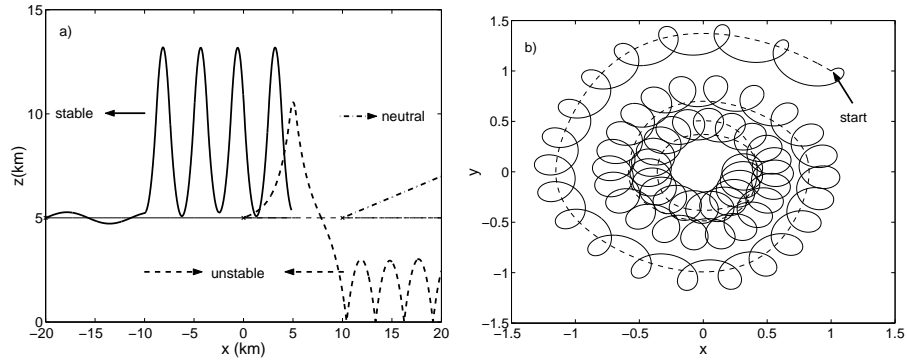


*Figure 1.* (a) Three trajectories are shown of parcel oscillations in the atmosphere for a given parcel energy. The stratification of the atmosphere is statically stable ( $d\theta/dz = \text{cst.} > 0$ ) for  $x < -10$  km, unstable ( $d\theta/dz = \text{cst.} < 0$ ) for  $-10 \text{ km} < x < 10$  km, and neutral (constant  $\theta$ ) for  $x > 10$  km and  $z < 10$  km, and isothermal and stable for  $z > 10$  km. The stable oscillations have a period of 10.84 min. When the atmosphere is hydrostatic, these oscillations disappear as the thin lines at  $z_r = 5$  km illustrate. (b) 41.7 days of (dimensionless) geostrophically balanced and unbalanced Hamiltonian motion of a particle in a simple, given Montgomery potential  $M_2(x, y)$  starting at  $(x, y) = (1, 1)$ . The predictability horizon lies around 14 days whereafter the balanced (dashed lines) and unbalanced (solid lines) trajectories depart from one another significantly.

## Hydrostatic primitive equations

The atmosphere is shallow for larger scales, and the aspect ratio  $\delta$  between vertical and horizontal length and velocity scales ( $D, W$  and  $L, U$ ) arises as a small parameter  $\delta = W/U \ll 1$ . At leading order in  $\delta$ , we find from the scaled version of system (1)–(4) the dynamics and

hydrostatic balance

$$\frac{d\mathbf{x}_h}{dt} = \mathbf{v} = \frac{\partial H_p}{\partial \mathbf{v}}, \quad (8)$$

$$\frac{d\mathbf{v}}{dt} = -\theta \nabla_h \Pi - f \hat{\mathbf{z}} \times \mathbf{v} = -\frac{\partial H_p}{\partial \mathbf{x}_h} - f \hat{\mathbf{z}} \times \frac{\partial H_p}{\partial \mathbf{v}}, \quad (9)$$

$$\frac{d\theta}{dt} = 0 \quad \text{and} \quad 0 = -\theta \partial \Pi / \partial z - g \quad (10)$$

with  $f = 2\Omega_3$ ,  $\hat{\mathbf{z}}$  the unit vector in the vertical direction, and the hydrostatic parcel energy

$$H_p(x, y, z, u, v, \theta, t) = (u^2 + v^2)/2 + M(x, y, z, t) \quad (11)$$

with Montgomery potential  $M = \theta \Pi(x, y, z, t) + g z$ . The vertical velocity  $dz/dt$  follows by insisting hydrostatic balance persists in time. We use these interim results next in the derivation of the conceptual  $1\frac{1}{2}$ - and 2-layer models.

## A $1\frac{1}{2}$ - and 2-layer atmosphere

Birner et al. (2002) measured the vertical temperature profiles which suggest a conceptual model with an isentropic troposphere and an isentropic or isothermal stratosphere. We therefore simplify the stratification of the atmosphere into an isentropic tropospheric layer and an isentropic or isothermal stratospheric layer, see Fig. 2(a). In this figure, we define the variables and constants used subsequently and denote their dependence, if any, on  $x, y$  and  $t$ .

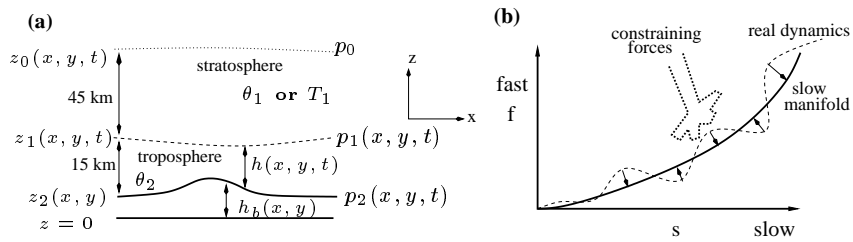


Figure 2. (a) Sketch of a simplified atmosphere with an isentropic troposphere and isentropic or isothermal stratosphere.  $p_0$  is a passive and constant pressure, and  $p_1$  and  $p_2$  are active pressures. (b) The slow manifold sketched has a third (or half) of the dimension of the entire Eulerian (or Lagrangian) phase space, with fast and slow variables  $f$  and  $s$ . Constraining forces, “the hand”, place the full dynamics on the manifold. When  $s$  and  $f$  are small, the dynamics is linear and separated in time such that  $f \rightarrow 0$ , as it is sketched.

Integrating hydrostatic balance  $\theta \partial \Pi / \partial z + g = 0$  in the tropospheric layer from  $z = z_2 = h_b$  to  $z$  with  $z_2 < z < z_1$ , we obtain the Montgomery potential

$$M_2(p_2) = \theta \Pi + g z = c_p \theta (p/p_r)^\kappa + g z = c_p \theta_2 (p_2/p_r)^\kappa + g h_b. \quad (12)$$

In an isentropic stratospheric layer one finds likewise, by integrating from  $z_1$  to  $z$  with  $z_1 < z < z_0$  and using (12) at  $z = z_1$  with  $p(x, y, z_1, t) = p_1$ , that

$$\begin{aligned} M_1(p_1, p_2) &= \theta \Pi + g z = g(z_0 - Z_0) = c_p \theta (p/p_r)^\kappa + g z \\ &= c_p (\theta_1 - \theta_2) (p_1/p_r)^\kappa + c_p \theta_2 (p_2/p_r)^\kappa + g(h_b - Z_0), \end{aligned} \quad (13)$$

while in an isothermal stratospheric layer, one obtains similarly

$$\begin{aligned} M_1(p_1, p_2) &= \theta \Pi + g z = g(z_0 - Z_0) = c_p \theta (p/p_r)^\kappa + g z \\ &= RT_1 \ln(p_1/p_0) + c_p \theta_2 ((p_2/p_r)^\kappa - (p_1/p_r)^\kappa) + g(h_b - Z_0). \end{aligned} \quad (14)$$

Note that, without any loss of generality, we have added a constant reference level  $Z_0$  to which we can fix the top of the stratospheric layer  $z_0$  at a later stage. Any initial  $z$ -independence in each layer remains intact, so only two parcels in a vertical column of fluid suffice for closure. Hence, the two-layer tropospheric-stratospheric model is the hydrostatic model (8)–(9) applied in each layer

$$\frac{d\mathbf{x}_\alpha}{dt} = \mathbf{v}_\alpha = \frac{\partial H_\alpha}{\partial \mathbf{x}_\alpha}, \quad (15)$$

$$\frac{d\mathbf{v}_\alpha}{dt} = -f \hat{\mathbf{z}} \times \mathbf{v}_\alpha - \nabla_h M_\alpha = -f \hat{\mathbf{z}} \times \frac{\partial H_\alpha}{\partial \mathbf{v}_\alpha} - \frac{\partial H_\alpha}{\partial \mathbf{x}_\alpha} \quad (16)$$

with  $\alpha = 1, 2$ ;  $\mathbf{x} = (x, y)_\alpha^T$  and parcel energy

$$H_\alpha(x_\alpha, y_\alpha, u_\alpha, v_\alpha, t) = (u_\alpha^2 + v_\alpha^2)/2 + M_\alpha(x_\alpha, y_\alpha, t). \quad (17)$$

Closure of these two-layer equations is reached via the layer pseudo-density

$$\sigma_\alpha(x, y, t) = \int_{D_{H_0}} \sigma_0(a, b) \delta(\mathbf{x} - \mathbf{x}'_\alpha(a, b, t)) da db \quad (18)$$

relating the horizontal label and position spaces with (using  $\partial p / \partial z = -\rho g$ )

$$dm = \rho dx dy dz = -dx dy dp / g = da db dc \quad (19)$$

$$\Delta m_2 = \sigma_2 dx dy = [(p_2 - p_1) / g] dx dy = \sigma_{2_0}(a, b) da db \quad (20)$$

$$\Delta m_1 = \sigma_1 dx dy = [(p_1 - p_0) / g] dx dy = \sigma_{1_0}(a, b) da db \quad (21)$$

$$\sigma_{\alpha_0} / \sigma_\alpha = \partial_x a \partial_y b - \partial_y a \partial_x b. \quad (22)$$

We emphasize that in each layer the Eulerian velocity is independent of depth, so  $\mathbf{v}_\alpha = \mathbf{v}_\alpha(x, y, t)$ . Hence  $\partial_z \mathbf{v}_\alpha$  remains zero once it was initially so.

Again, we can derive continuity equations  $\partial_t \sigma_\alpha + \nabla_h \cdot (\sigma_\alpha \mathbf{v}_\alpha) = 0$  and a materially conserved PV:  $dQ_\alpha/dt = 0$  with

$$Q_\alpha = (f + \hat{\mathbf{z}} \cdot \nabla \times \mathbf{v}_\alpha) / \sigma_\alpha.$$

**$1\frac{1}{2}$ -layer models.** When the stratospheric layer is much deeper than the tropospheric layer, *e.g.*, 45 km versus 15 km, we approximate the top  $z_0$  to  $Z_0$  and neglect the motion in the stratospheric layer. Thus, from (13) or (14) one finds  $M_1(p_1, p_2) = 0$ . The stratospheric pressure  $p_1$  remains active, but the dynamics [(15) and (16) for  $\alpha = 2$ ] is evolved in the tropospheric layer. The bottom pressure  $p_2$  used to define  $M_2$  [(12)] in the tropospheric momentum equations (16) is then determined from  $\sigma_2 = (p_2 - p_1)/g$  and  $M_1(p_1, p_2) = 0$ .

**Static stability.** Static stability means that a fluid parcel perturbed in the vertical oscillates around a certain height with the Brunt-Väisälä frequency  $N$  rather than taking off. The eigen-values  $a$  of the  $1\frac{1}{2}$ -layer equations [(15) and (16) for  $\alpha = 2$  with  $\sigma_2 = (p_2 - p_1)/g$  and  $M_1(p_1, p_2) = 0$ ] are

$$a^2 \propto \begin{cases} c_p \kappa (\theta_1 - \theta_2) (p_1/p_r)^{\kappa-1} (p_2 - p_1)/p_r & (\theta_2 - \theta_1\text{-model}) \\ (p_2 - p_1) (p_r R T_1 / p_1 - c_p \theta_2 \kappa (p_1/p_r)^{\kappa-1}) & (\theta_2 - T_1\text{-model}). \end{cases} \quad (23)$$

These eigen-values are real when the atmosphere is statically stable or  $d\theta/dz > 0$ : this occurs when  $\theta_1 > \theta_2$  in the  $\theta_2 - \theta_1$ -model, and when  $T_1 > \theta_2 (p_1/p_r)^\kappa$  in the  $\theta_2 - T_1$  model. While the  $\theta_2 - \theta_1$  model remains statically neutral or stable if it is initially so, the stability of the  $\theta_2 - T_1$  model thus depends on  $p_1(x, y, t)$ .

## 2. Linear Modes

Linearized around a “rest depth”  $H$  with  $\sigma = \sigma_2 = H(x, y) + \eta$ , the  $1\frac{1}{2}$ -layer models [(15) and (16) for  $\alpha = 2$ ] become

$$\partial_t \mathbf{v} = -f \hat{\mathbf{z}} \times \mathbf{v} - g' \nabla_h \eta \quad \text{and} \quad \partial_t \eta + \nabla_h \cdot (H \mathbf{v}) = 0 \quad (24)$$

with velocity  $\mathbf{v} = \mathbf{v}'_2$  and effective gravity  $g'$ . This linearized system is akin to the classical, linearized shallow water equations with (for  $h_b = 0$ )

$$g' \propto \begin{cases} \frac{(\theta_1 - \theta_2) P_1^{\kappa-1}}{(\theta_1 - \theta_2) P_1^{\kappa-1} + \theta_2 P_2^{\kappa-1}} & (\theta_2 - \theta_1\text{-model}) \\ \frac{p_r R T_1 / P_1 - c_p \kappa \theta_2 (P_1/p_r)^{\kappa-1}}{R T_1 / P_1 + c_p \kappa \theta_2 (P_2^{\kappa-1} - P_1^{\kappa-1})} & (\theta_2 - T_1\text{-model}) \end{cases} \quad (25)$$

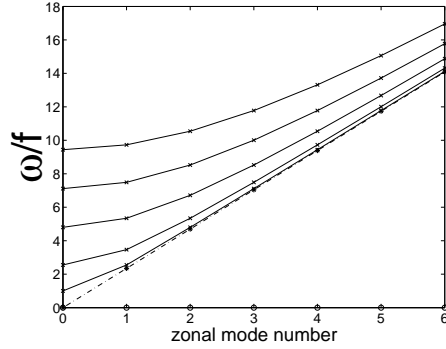


Figure 3. Dispersion relation of linear modes in a periodic channel for the  $\theta_2$ - $\theta_1$ -model.

and the rest state  $H = (P_2 - P_1)/g$ , which is consistent with (23). In a periodic channel with constant  $H$ , the linear modes using  $\eta \propto e^{i(kx + \omega t)}$  ( $i^2 = -1$ ) consist of: a vortical or geostrophic mode with frequency  $\omega = 0$ , Poincaré GW modes with  $\omega^2 = f^2 + g' H (k^2 + l^2)$ , and counterclockwise propagating boundary-trapped Kelvin modes with  $\omega^2 = g' H k^2$  (for constant  $f > 0$ ). We observe in the dispersion diagram in Fig. 3 that there is a time-scale separation between the vortical and GW modes, except perhaps for the lowest-order Kelvin modes and the geostrophic solution.

As usual, a linear mode analysis is limited in scope. First, the dynamics is nonlinear, so there is no clear notion of a time scale separation anymore. Nonlinear “slow” dynamics can have high-frequency overtones triggering resonances or interactions with “fast” dynamics. Second, approaching the equator, the effective Coriolis parameter  $f \rightarrow 0$ , giving rise to equatorial Kelvin waves and mixed Rossby-gravity waves or mixed slow-fast linear modes. Consequently, linear Kelvin or gravity mode solutions of larger amplitude used as initial condition, can develop vortex motion and, vice versa, linear geostrophic or Rossby modes can develop GW motion from instabilities. Mixed fast-slow motion emerges in simulations, see Fig. 4, of the nonlinear evolution of a linear Kelvin mode solution in a zonally periodic channel used as initial condition. In particular PV is constant (in time and/or space) for a Kelvin or Poincaré mode,

$$Q_2 = Q = (f + \hat{\mathbf{z}} \cdot \nabla \times \mathbf{v})/\sigma = f/H \quad \text{and} \quad \partial_t Q + (\mathbf{v} \cdot \nabla_h)Q = 0, \quad (26)$$

before the occurrence and parameterization of wave breaking. These constant PV regions are then distinguished, ideally, from regions where

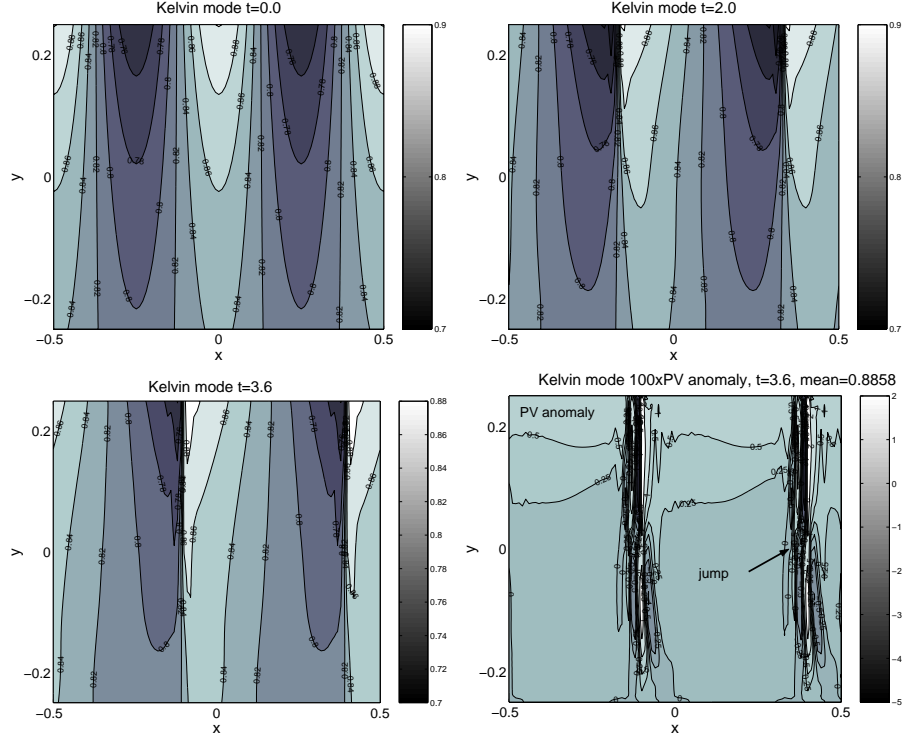


Figure 4. Top: contour plots of  $\sigma$  in simulations of the 1.5-layer  $\theta_2$ - $\theta_1$ -model with shock-capturing numerics which, however, do not conserve absolute vorticity  $\sigma Q$ . Bottom: simulations displaying  $\sigma$  (left) and  $100\times$  PV anomaly ( $Q - f/H$ ) (right) at the final time. Non-dimensional quantities are displayed, for example in a domain of  $4000 \times 2000$  km with  $z_1 \approx 15$  km and  $Z_0 \approx 60$  km.

a wave breaking parameterization generates non-constant PV anomalies  $Q - f/H$  (*cf.*, Peregrine and Bokhove, 1998).

### 3. Balanced Dynamics

The concept of balanced large-scale flow arises from the observation that at mid-latitudes the atmosphere and oceans are in approximate geostrophic balance, and near the equator the Earth's rotation remains influential. Locally — due to topography, strong (tropical) convection, dissipative and non-dissipative (GW) instabilities — balance often fails. The notion of balance may be formalized in various ways: small Rossby and Froude numbers are identified from measurements, observations or simulations, and then used in scaling arguments. Subsequently, a perturbative or iterative approach is applied to approximate the full or parent

model. The resulting dynamics evolves on a slow or slaving manifold of reduced dimensionality, see the sketch in Fig. 2(b).

The preservation of certain conservation laws, or the variational or Hamiltonian structure, may be imposed heuristically in these balanced approximations. Whether the conservative or non-conservative approach to balanced dynamics is better, remains undecided and depends on the, perhaps subjective, value placed on (point-wise) accuracy, and long-term stability.

Geostrophic balance denotes the alignment of the wind vectors along the pressure or Montgomery potential isobars. To derive this leading order balance, we rewrite the  $1\frac{1}{2}$ -layer equations [(16) for  $\alpha = 2$ ] and drop the layer subscripts

$$\frac{du_i}{dt} = \frac{f}{R} \epsilon_{ij} u_j - \frac{1}{R} \partial_{x_i} M = \frac{f}{R} \epsilon_{ij} \frac{\partial H}{\partial u_i} - \frac{1}{R} \frac{\partial H}{\partial x_i} \quad (27)$$

with the permutation symbol  $\epsilon_{ij}$ ,  $\mathbf{v} = (u_1, u_2)^T$  and  $i, j = 1, 2$ . The Rossby number  $R = U/(fL) \ll 1$  is placed in (27) at the relevant locations, as the ratio of the GW time scale  $1/f$  and the vortical time scale  $L/U$  with typical length and velocity scales  $L$  and  $U$ . At leading order in  $R$ , we find geostrophic balance from (27) as a constraint on the velocity with  $M/f$  being a stream function in the balance relations  $u = -\partial_y M/f$  and  $v = \partial_x M/f$ . In general, (higher-order) velocity constraints obtain the form

$$\phi_i = u_i - u_i^C[\sigma(\mathbf{x})] \stackrel{e.g.}{=} u_i + \frac{1}{f} \epsilon_{ij} \partial_{x_j} M, \quad (28)$$

in which  $u^C[\sigma]$  operates (non-locally) on  $\sigma$  and, hence, through  $\sigma$  on the parcel coordinates  $x$  and  $y$ . Next, we use these constraints to derive balanced models.

### Conservative balanced models: slaved Hamiltonian approach

We illustrate the derivation of Hamiltonian balanced models in the hybrid parcel framework. The variables  $(x_i, u_i)$  are transformed to  $(x_i, \phi_i)$  using (28), and a constrained variational derivative is introduced

$$\left. \frac{\partial H}{\partial x_i} \right|^C = \frac{\partial H}{\partial x_i} + \frac{\partial H}{\partial u_j} \frac{\partial u_j^C}{\partial x_i}, \quad (29)$$

where  $(\cdot)|^C$  denotes that  $\phi_i = 0$  in derivatives of  $x$  and  $y$ . The evolution on the slow manifold of reduced dimensionality becomes, using (15)

and (16),

$$\frac{dx_i}{dt} = \frac{\partial H}{\partial u_i} = u_i \quad \text{and} \quad 0 = \frac{d\phi_i}{dt} = -\frac{\partial H^C}{\partial x_i} + \epsilon_{ij}\sigma Q^C u_j \quad (30)$$

with  $\sigma Q^C = f + \partial v^C / \partial x - \partial u^C / \partial y$ . The slaved Hamiltonian dynamics on the slow manifold is concisely written as

$$\frac{dx_i}{dt} = (L^{-1})_{ij} \frac{\partial H^C}{\partial x_j} \quad \text{or} \quad \frac{dF^C}{dt} = \frac{\partial F^C}{\partial x_i} (L^{-1})_{ij} \frac{\partial H^C}{\partial x_j} \quad (31)$$

[*cf.* Dirac (1958)] with skew-symmetric matrix  $L_{ij} = \epsilon_{ij}\sigma Q^C$  and arbitrary function  $F^C = F^C(x, y)$  and  $H^C = H(x, y, u^C, v^C)$ . Simplified numerical integrations are explained in Fig. 1(b). It is unclear whether the parcel balanced dynamics (31) presented is a didactic simplification, or equivalent to the results for the Eulerian balanced equations in Vanneste and Bokhove (2002).

#### 4. Wave-Vortex Interactions and Numerical Schemes

The parameterization of unresolved gravity waves is a critical component in numerical GCMs. Gravity waves can influence the large-scale dynamics in various ways: (i) breaking gravity waves dissipate energy to small scales and deposit momentum to drive the mean, large-scale flow (McFarlane, 1987); (ii) instabilities of balanced vortical flows locally excite gravity waves, which can transport energy and momentum away (Vanneste and Yavneh, 2004); and (iii) non-dissipative wave-vortex interactions, such as remote recoil, can lead to a cumulative forcing of the mean vortical flow (Bühler and McIntyre, 2003). The crucial question is how to parameterize these unresolved GW-effects, studied hitherto in isolation, in numerical models for large-scale flows on advective time scales, given the resolved large-scale flow.

New numerical schemes have emerged with a focus on improved meshes without pole problem, conservation properties and advection-dominated time integration. Based on gas dynamics and novel finite-element discretizations (Bokhove, 2005; Fig. 4), an impulse formulation of the  $\theta$ - $T$ -model with 3 prognostic equations can be used, which are shock-capturing but with explicit time stepping limited by the largest GW speed. In atmospheric dynamics, the velocity formulation with 3 prognostic equations is often preferred (Ringler and Randall, 2002). The GW speed is then still the limiting factor. Hamiltonian Particle Mesh methods (HPM) involve (15)–(18) with 4 prognostic equations and 1 integral equation (Frank and Reich, 2003). By smoothing the pseudo-density,

time step restrictions can be lifted. To emphasize the vortical dynamics, a mass-divergence-vorticity formulation is used by Thuburn (1997) and Ringler and Randall (2002) resulting in 3 prognostic and 2 elliptic equations. The advective time step is then used after some numerical stabilization. The approaches by Ringler and Randall conserve mass, energy, potential enstrophy and vorticity. Mass or PV conserving balanced models consist of a prognostic equation and 2–4 elliptic equations of the first and second order. These elliptic inversions are time consuming and require special (multi-grid) techniques.

## 5. Conclusions

The HPM and related semi-Lagrangian numerical schemes, as well as the ones using vorticity-divergence variables (Frank and Reich, 2003; Thuburn, 1997; and Ringler and Randall, 2002) seem to be most advantageous as they use the larger advective time step, at the expense of introducing an artificial numerical GW-vortex parameterization. It may be a good strategy to test GW-vortex parameterizations in both the balanced models and high-resolution (in space and time) primitive equations. Otherwise, it is unclear to what extent the (artificial) numerical GW parameterizations in the numerical schemes jeopardize the physical ones. Clearly, the potential interplay between physical and (hidden) numerical parameterizations of gravity waves is a research question with important implications for GCMs. Finally, a thorough answer to the initial question whether a balanced model can provide accurate climate predictions needs to be postponed, although Olaguer’s (2002) results seem to be encouraging.

## Acknowledgments

The criticism of J. Frank and B.J. Geurts has been much appreciated. The  $\theta$ - $T$ -model originates from an unpublished work with W.T.M. Verkley.

## References

- T. Birner, A. Dörnbrack and U. Schumann. How sharp is the tropopause at midlatitudes? *Geophys. Res. Lett.* **29**: 10.1029, 2002.
- O. Bokhove. Flooding and drying in finite-element discretizations of shallow-water equations. Part 1: One dimension. *J. Sci. Comput.* **22**, To be published, 2005.
- O. Bokhove and W.T.M. Verkley. Constrained isentropic models of tropospheric dynamics. Submitted to *Quart. J. Roy. Meteor. Soc.*, 2004.
- O. Bühler and M.E. McIntyre. Remote recoil: a new wave-mean interaction effect. *J. Fluid Mech.* **492**, 207–230, 2003.

- P.A.M. Dirac. Generalized Hamiltonian dynamics. *Proc. Roy. Soc. Lond. A* **246**, 326–332, 1958.
- M. Dixon and S. Reich. Symplectic time-stepping for particle methods. *GAMM*, to appear, 2004.
- J. Frank and S. Reich. Conservation properties of smoothed particle hydrodynamics applied to shallow water equations. *BIT* **43**, 40–54, 2003.
- N.A. McFarlane. The effect of orographically excited gravity wave drag on the general circulation of the lower stratosphere and troposphere. *J. Atmos. Sci.* **44**, 1775–1800, 1987.
- E.P. Olaguer. An efficient 3-D model for global circulation, transport and chemistry. *IMA Vol. Math. Appl.* **130**, 205–276, 2002.
- D.H. Peregrine and O. Bokhove. Vorticity and surf zone currents. *Proceedings of the 26th International Conference on Coastal Engineering 1998, ASCE, Copenhagen*. 745–758, 1998.
- T.D. Ringler and D.A. Randall. A potential enstrophy and energy conserving numerical scheme for solution of the shallow-water equations on a geodesic grid. *Mon. Wea. Rev.* **130**, 1397–1410, 2002.
- J. Thuburn. A PV-based shallow-water model on a hexagonal-icosahedral grid. *Mon. Wea. Rev.* **125**, 2328–2347, 1997.
- J. Vanneste and O. Bokhove. Dirac-bracket approach to nearly-geostrophic Hamiltonian balanced models. *Physica D* **164**, 152–167, 2002.
- J. Vanneste and I. Yavneh. Exponentially small inertia-gravity waves and the breakdown of quasi-geostrophic balance. *J. Atmos. Sci.* **61**, 211–223, 2004.